Editors' Suggestion | Featured in Physics

Experimental Demonstration of Laser Guiding and Wakefield Acceleration in a Curved Plasma Channel

Xinzhe Zhu,[1,*] Boyuan Li,[1,2,3,*] Feng Liu,[1,2,†] Jianlong Li,[1] Zewu Bi,[1] Xulei Ge,[1,2] Hongyang Deng,[4] Ziyang Zhang,[4] Peilin Cui,[5] Lin Lu,[1,2] Wenchao Yan,[1,2] Xiaohui Yuan,[1,2] Liming Chen,[1,2] Qiang Cao,[4] Zhenyu Liu,[5] Zhengming Sheng,[1,2,3] Min Chen,[1,2,‡] and Jie Zhang[1,2,3,§]

[1]*Key Laboratory for Laser Plasmas (Ministry of Education), School of Physics and Astronomy, Shanghai Jiao Tong University, Shanghai 200240, China*

[2]*Collaborative Innovation Center of IFSA (CICIFSA), Shanghai Jiao Tong University, Shanghai 200240, China*

[3]*Tsung-Dao Lee Institute, Shanghai Jiao Tong University, Shanghai 200240, China*

[4]*The Institute of Technological Sciences, Wuhan University, Wuhan 430072, China*

[5]*School of Mechanical Engineering, Shanghai Jiao Tong University, Shanghai 200240, China*

(Received 27 November 2022; revised 24 February 2023; accepted 7 April 2023; published 23 May 2023)

Curved plasma channels have been proposed to guide intense lasers for various applications, such as x-ray laser emission, compact synchrotron radiation, and multistage laser wakefield acceleration [e.g. J. Luo *et al.*, Phys. Rev. Lett. **120**, 154801 (2018)]. Here, a carefully designed experiment shows evidences of intense laser guidance and wakefield acceleration in a centimeter-scale curved plasma channel. Both experiments and simulations indicate that when the channel curvature radius is gradually increased and the laser incidence offset is optimized, the transverse oscillation of the laser beam can be mitigated, and the stably guided laser pulse excites wakefields and accelerates electrons along the curved plasma channel to a maximum energy of 0.7 GeV. Our results also show that such a channel exhibits good potential for seamless multistage laser wakefield acceleration.

DOI: 10.1103/PhysRevLett.130.215001

Laser wakefield acceleration (LWFA) can provide acceleration gradients as high as GV/cm, making it promising for compact accelerators and radiation sources [1–6]. GeV-level energy gain at the centimeter scale has been routinely achieved [7–9], and 8-GeV electron bunches have also been demonstrated using longer plasma channels [10]. However, higher-energy applications such as electron-positron colliders require particles with hundreds of GeV to TeV energy [11–13]. This exceeds the expected energy gain in a single LWFA stage owing to the pump depletion of the drive lasers and the acceleration dephasing of the electrons. To overcome this limitation, a multistage LWFA with successive fresh laser drivers is necessary.

Several schemes have been proposed for staged LWFA [14–16]. The first experimental demonstration was performed by Steinke *et al.* at the LBNL [17]. In their scheme, a fresh intense drive laser was injected into the second acceleration stage using a plasma mirror [18]. To overcome the spatial dispersion of the electron beam between stages, an external plasma lens was used to refocus the accelerated electrons before they were injected into the second stage [19]. A capture efficiency of approximately 3.5% and an energy gain of approximately 100 MeV in the second stage were observed. Another scheme without a plasma mirror and plasma lens was theoretically proposed by Luo *et al.* [20], where a curved plasma channel with varying curvature is proposed to stably guide the intense fresh laser pulse to the second stage. Theoretical studies show that a capture efficiency close to 100% is feasible because electrons can be self-guided in a straight plasma channel, which makes the scheme very promising for efficient multistage acceleration. Although the guidance of relativistic lasers in straight plasma channels and subrelativistic lasers in curved capillaries with a fixed curvature has been experimentally demonstrated [21], both theoretical and experimental studies have also revealed that strong transverse oscillations of laser pulses are easily developed during laser propagation [22]. Even though a special curved plasma channel proposed may mitigate such transverse oscillations [20], it has not yet been verified experimentally.

In this Letter, we present an experimental study of the stable propagation of relativistically intense lasers in a curved plasma channel with varying curvatures. Optical diagnosis and particle-in-cell (PIC) simulations indicate that the usual transverse oscillations of the laser beam centroid can be avoided when an appropriate laser off-axis incidence at the entrance of the curved channel is used. GeV-level electron acceleration by the guided laser pulse in the curved channel was experimentally observed, indicating that such a plasma channel is promising for future staged wakefield acceleration.

The curved channel was fabricated by pasting two planar sapphire crystals with half-groove structures that

were machined using femtosecond laser pulses; see Supplemental Material [23] for detailed information of capillary fabrication which includes Refs. [24–26]. The channel has a transversely cylindrical shape with an inner diameter of 500 μm and a longitudinal profile with two parts: a curved section and a straight section with lengths of 22 and 8 mm, respectively. The capillary configuration is shown in Fig. 1. The curvature radius of the curved section gradually increased from $R = 6$ cm to $R = \infty$, which yielded a tangential deflection angle of 10.4° between its entrance and exit axes. The curved section is followed by a straight section. The capillary was filled with helium gas and discharged at 18 kV from both ends. As shown in Fig. 1(a), the gas inlets were arranged symmetrically near both ends of the capillary. With this configuration, the fluid simulations performed by Ansys Fluent [27] showed a nearly uniform gas-density distribution along the channel axis. The density profile could be adjusted linearly by tuning the gas pressure. After discharge, the plasma density was measured using the Stark spectra broadening method, where the helium characteristic line ($\lambda_{\mathrm{He}} \sim 587.6$ nm) was used [28]. Experimental studies have shown that a plasma channel can be formed within ±50 ns around the peak of the discharge current. Figure 1(b) shows a typical radial density distribution of the plasma channel detected at the capillary entrance when the gas pressure was one bar. The density profile can be approximated by a parabolic function $n(r) = n_0 + \Delta n r^2/r_0^2$ with $n_0 = 5.6 \times 10^{17}$ cm^{-3}, $\Delta n(\mathrm{cm}^{-3}) = 1.13 \times 10^{20}/r_0^2$ (μm), and $r_0 = 53$ μm.

It is known that for a straight plasma channel, a laser beam can stably propagate with a constant spot size when its radius is matched with the plasma channel, i.e., $w_0 = r_0$ [29]. However, to guide a relativistic laser for a staged LWFA, the laser should first be injected into the curved part and then propagate inside the straight part, as shown in Fig. 1(a). However, laser guidance has not been fully investigated. We performed experimental studies on a 200 TW Ti: sapphire ($\lambda_L = 800$ nm) laser facility at the Shanghai Jiao Tong University. The laser pulse had a duration of $\tau = 30$ fs (FWHM) and an energy of 3 J. It was focused by a $f/20$ off-axis parabolic mirror onto a spot with a radius of $w_0 = 28$ μm. Figure 1(c) shows the experimental setup for laser guiding and electron beam diagnosis. The laser spot at the channel exit was imaged using a charge-coupled device (CCD). The pulse energy was kept below 10 mJ and the intensity at 3×10^{15} W/cm^2 during the laser-guiding experiment to avoid damaging the optics.

Figure 2(a) shows the laser-beam profile at the capillary entrance. Experiments show that when such a laser beam is injected into the capillary, it cannot be well guided if the injected laser axis is too close to the channel center. As shown in Fig. 2(b), most of the beam energy was lost or dispersed in the capillary, and the output beam spot severely deviated from a Gaussian profile. This is because the laser oscillates transversely in a curved channel [21], which breaks the pulse front when the laser oscillates in the high-density region. To achieve a stable guidance, the transverse oscillation of the laser pulse must be mitigated. For a curved plasma channel with a fixed curvature R, theoretical analysis shows that the laser can propagate without transverse oscillation when it is injected with an offset distance of $r_{\mathrm{os}} = (n_{\mathrm{cr}}/\Delta n) w_0^2/R$, where r_{os} is the offset distance from the channel axis and n_{cr} is the critical plasma density of the laser. However, if r_{os} remains constant along the curved part, the guided pulse is injected

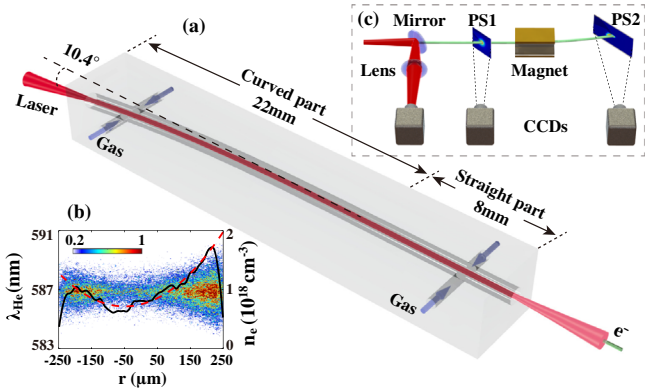

FIG. 1. (a) Structure of the discharged capillary to produce the curved and straight plasma channel. (b) Spectrum distribution and calculated profile of the plasma density along the radial direction at the entrance of the discharged capillary. (c) Experimental setup for the measurements of laser guiding and electron acceleration.

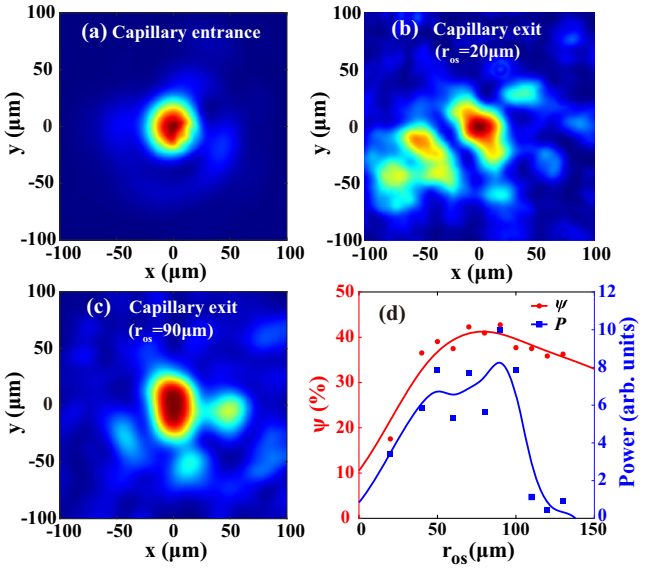

FIG. 2. Laser guiding at 3×10^{15} W/cm^2 in the curved plasma channel. (a) Beam spot at the capillary entrance. (b) and (c) Beam spots at the capillary exit for $r_{\mathrm{os}} = 20$ and $r_{\mathrm{os}} = 90$ μm, respectively. (d) Dependence of energy concentration (Ψ) and transmitted power (P) on the offset distance r_{os}, the fitted smoothing spline curves show their evolution tendency.

off-axis into the straight part of the channel, which induces transverse laser centroid oscillations in the straight channel. To prevent this and smoothly guide the laser in the entire plasma channel, a capillary with a gradually varying curvature was proposed [20]. Theoretical and numerical simulation studies have shown that such a channel can stably guide the laser pulse and is suitable for staged LWFA.

We studied laser guidance by checking the evolution of the output laser spot with the incidence offsets. Figure 2(c) shows the laser spot at the capillary exit at $r_{\mathrm{os}} = 90$ μm. With such an offset, the laser spot at the exit shows a similar size to the one at the entrance. In contrast, the beam profile deformed severely when the laser was injected near the axis into the channel, as shown in Fig. 2(b). We found that the beam quality of the guided laser has a strong correlation with r_{os}. Two quantities were used to evaluate the guiding performance: the transmitted laser power in spot at the exit $[P = \iint_0^{x^2+y^2\le w_0^2} I(x,y)dxdy]$ and energy concentration of the beam $[\Psi = P/\iint_0^{\infty} I(x,y)dxdy]$. Figure 2(d) shows the evolution of these two quantities with the incidence offset (r_{os}). It can be observed that both Ψ and P are small when the laser is injected close to the channel axis. As r_{os} increases, the laser beam begins to propagate in the plasma channel without significant diffraction, and the transmission efficiency increases, which is a trend similar to the simulations where the transverse oscillations and the induced laser front deformation were found to be suppressed. However, when the offset distance continuously increases, the laser guiding worsens, and the simulation shows that the laser experiences a stronger transverse oscillation in the straight channel. This was confirmed by our ray-tracing simulations [see Fig. 4(a)]. In our experiments, Ψ and P reached a maximum at $r_{\mathrm{os}} = 90$ μm, indicating that the laser beam was guided both in the curved and straight plasma channels under this condition, where the output Gaussian beam profile can be observed, as shown in Fig. 2(c). However, even though the core part of the laser spot appears much better conserved, one can still see the side shadows and islands around the main spot. This means that there is still plenty of room to improve the guiding further. This imperfection may be caused by the imperfect symmetry of the capillary as shown in the Supplemental Material [23]).

We further studied relativistic laser guidance and wakefield acceleration in a curved plasma channel. Experiments show that around the optimal incidence condition, a high-quality energetic electron beam can also be detected. In the acceleration experiments, helium gas mixed with 0.5% nitrogen was used to trigger ionization injection. The laser energy was increased to full energy (3J), which corresponds to a normalized laser amplitude of $a_0 \approx 1$, where a_0 is related to the laser intensity I by $a_0 = [I(\mathrm{W/cm^2})\lambda^2(\mu\mathrm{m})/1.37\times10^{18}]^{1/2}$. The setup for the

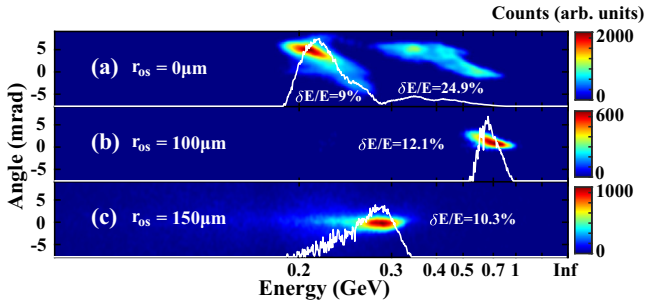

FIG. 3. Electron bunches obtained by laser wakefield acceleration in the curved plasma channel with different laser incidence offsets. (a,b,c) correspond to offsets of 0, 100 and 150 μm, respectively. The spatially integrated energy spectrum (dN/dE) and relative root-mean-squared (rms) energy spreads ($\delta E/E$) of each bunch are marked on the graph.

electron measurement is shown in Fig. 1(c). The electron beams are first monitored by a phosphor screen (PS1) to diagnose its profile and pointing. Subsequently, the energy spectra were resolved using PS2 with a permanent magnet of 1 T. In the experiments, we found that the pointing of the accelerated electrons is roughly the same as the axial direction of the straight channel, the pointing fluctuations in the horizontal and vertical directions are 0.73 and 0.53 mrad, respectively. Such electron pointing clearly indicates that the laser has been guided further in the straight section. Typical electron spectra with different offset distances of laser incidence are shown in Fig. 3. The deconvoluted spectra calculated from the raw data are labeled by the white curves. The maximum central energy of the electron bunch (~0.7 GeV) is observed when $r_{\mathrm{os}} = 100$ μm. In the case where $r_{\mathrm{os}} = 0$ and 150 μm, lower-energy electrons (0.2–0.3 GeV) were observed in the spectra.

It can be observed that the bunch number of the accelerated electrons also varies with the offset of the laser incidence. For a small r_{os}, multiple electron bunches are observed, and the corresponding energy spread is larger, as shown in Fig. 3(a). When r_{os} increases from 0 to 100 μm, the lower-energy electron bunch disappears and the energy spread of the higher-energy bunch is simultaneously reduced, as shown in Fig. 3(b). For even larger r_{os}, the higher-energy bunch disappears, only low-energy electron bunches can be observed, as shown in Fig. 3(c).

To roughly estimate the dependence of the laser guidance on the laser incidence, ray-tracing simulations for laser propagation were performed using the ZEMAX code [30]. The input light rays in the simulations were initially focused at the entrance of the plasma channel, with the same f number used in the experiments. Three simulations with different laser offsets ($r_{\mathrm{os}} = 0, 100, 150$ μm) were investigated. The trajectories of the laser centroids are presented in Fig. 4(a) with dashed lines. This shows that when the laser incidence offset was 100 μm, the transverse oscillation of the laser pulse was the smallest. The laser

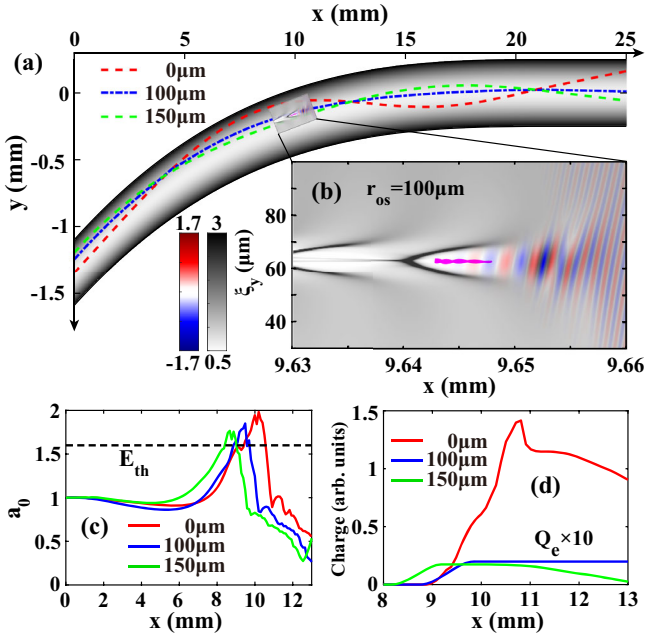

FIG. 4. Simulation results of laser evolution, wakefield generation, and electron acceleration. (a) The dashed curves represent the simulated trajectories of the laser centroid from ray tracing for different laser incidence offsets. (b) Spatial distributions of laser fields and electron density when the laser propagates to 9.6 mm with $r_{os} = 100$ μm, where electrons located in the first plasma wave bucket with energy higher than 10 MeV are marked with magenta dots. (c) Evolution of laser intensity (a_0), where the black dotted line represents the threshold electric field (E_{th}) for N^{5+} ionization. (d) Evolution of electron charge in the trapped bunches for different laser offsets, where the beam charge for the case of $r_{os} = 100$ and 150 μm should be multiplied by a factor of 10.

pulse gradually settles down and propagates along the central axis of the curved channel, after which it stably enters the straight channel, whereas the laser pulses with 0 and 150 μm offsets experience stronger oscillations. During propagation and oscillation, the laser alternately reaches the higher- and lower-density regions, and its direction is deflected several times. With such large-amplitude oscillations, the pulse breaks its integrity, and both wakefield and injected electrons are severely affected, leading to unstable electron acceleration.

To study the detailed processes of laser guiding, wakefield generation, and electron acceleration, PIC simulations were performed using the code OSIRIS [31]. Owing to computational limitations, a full simulation of the entire channel is impossible. Because the most critical parts for laser propagation, wake excitation, and electron injection occur in the curved part of the channel, PIC simulations were focused on the first section (0 mm $< x <$ 13 mm). A moving window is set along the channel direction, and the transverse position of the window is represented by $\xi_y = y_{\text{window}} - y_{\text{axis}}$, where y_{window} is the position in the lab frame and y_{axis} is the position of the capillary central axis. A typical snapshot of the laser and wakefield (electron density) profile at point $z = 9.6$ mm for $r_{os} = 100$ μm is plotted in Fig. 4(b). For a clear visualization, the electron density n_e' in the figure deducts the central electron density at that location (i.e., $n_e' = n_e - n_0$).

Figures 4(c) and 4(d) show the evolution of the normalized laser amplitude a_0 and the accelerated electron charge along the channel, respectively. The simulation results show that a large number of electrons are injected when the laser electric field exceeds the ionization injection threshold of N^{5+} ($a_0 \approx 1.6$) at approximately $x = 8$ mm. In the experiment, the initial laser peak amplitude was $a_0 \approx 1$, which is lower than the ionization injection threshold. In addition, the laser width 28 μm was smaller than the matched width of the channel (53 μm). When the laser is incident into the plasma channel with an incidence offset of $r_{os} = 0$ μm, in addition to the transverse centroid motion, the laser also experiences transverse defocusing and focusing. When the pulse approaches the high-density region, it is transversely compressed [see the red dashed line in Fig. 4(a)]. A higher laser intensity then forms with a peak $a_0 = 2.0$, leading to ionization injection around $x = 9$–11 mm. In the case of $r_{os} = 150$ μm, a similar process occurs in the simulation, but ionization occurs earlier and the injection only lasts for a short period. An excessive laser offset shrinks the ionization injection length, and the injected electrons experience stronger oscillations owing to the asymmetric transverse fields of the wake, resulting in severe electron loss, and only a few electrons can be guided to the straight part of the channel.

The observed electron energy spectra also revealed the evolution of the laser and electrons. When the laser is incident at $r_{os} = 0$ μm, electrons are injected twice, resulting in two electron bunches in the spectrum. When the laser is incident with $r_{os} = 100$ μm, electrons are injected at an earlier time, and a higher-energy electron bunch with an energy of 0.7 GeV is observed. The low dark current also indicates that the laser propagated smoothly in the following region. When the laser is incident at $r_{os} = 150$ μm, the simulation shows that it experiences severe transverse oscillations after entering the curved plasma channel. Although electrons are injected via ionization injection even earlier than in the other two cases, they are lost before entering the straight channel, as shown by the green line in Fig. 4(d). Only electrons injected at the second time (not shown here, it is close to the straight channel, $x > 13$ mm) can be successfully accelerated in the straight channel. They form a low-energy peak in the spectrum, as shown in Fig. 3(c).

In the above simulations, we found that less than 0.5% of the accelerated electrons were self-injected. The energy of these electrons (10–30 MeV) indicate that they do not gain sufficient acceleration in the wakefield. Experiments and simulations with pure helium gas were also performed, where it is found that the charge of self-injected electrons is much lower than the ionization injected electrons.

The small amount of self-injection indicates that the curved channel could be used to only guide the laser without wakefield acceleration by using pure helium gas, which is favorable for the curved plasma channel-based staged LWFA scheme to avoid dark current.

In conclusion, we have shown experimental evidences that a discharged curved capillary with varying curvature can be used to guide intense lasers and accelerate electrons to sub-GeV energy. Both experiments and simulations showed that the transverse oscillation of the laser pulse can be suppressed by choosing appropriate incidence offsets. The laser-guiding results demonstrated that the laser can maintain its shape without significant distortions, and 43% of the energy was constrained within the initial laser spot size. The LWFA results showed that high-amplitude wake fields were excited and ionization injection was triggered in this curved plasma channel, where the electrons were accelerated to 0.7 GeV with quasi-monoenergetic spectrum. Pure laser guidance in a curved channel without electron injection and acceleration is also possible when pure helium gas is used. Such curved plasma channels are applicable not only for staged LWFA [32], but also for other potential applications such as electron beam bending for synchrotron radiation [33,34], as well as active plasma lenses for charged particle focusing and guiding [35,36].

This work was supported by the National Natural Science Foundation of China (Grants No. 11991074 and No. 12225505) and the Strategic Priority Research Program of the Chinese Academy of Sciences (Grants No. XDA25010500 and No. XDA25050000). The simulations were performed at the π Supercomputer Center at SJTU. The authors would like to acknowledge the OSIRIS Consortium, consisting of UCLA and IST (Lisbon, Portugal) for providing access to the OSIRIS 4.0 framework.

*These authors contributed equally to this work.
†liuf001@sjtu.edu.cn
‡minchen@sjtu.edu.cn
§jzhang1@sjtu.edu.cn

[1] T. Tajima and J. M. Dawson, Phys. Rev. Lett. **43**, 267 (1979).
[2] E. Esarey, C. B. Schroeder, and W. P. Leemans, Rev. Mod. Phys. **81**, 1229 (2009).
[3] S. Kneip, C. McGuffey, J. L. Martins, S. F. Martins, C. Bellei, V. Chvykov, F. Dollar, R. Fonseca, C. Huntington, G. Kalintchenko *et al.*, Nat. Phys. **6**, 980 (2010).
[4] C. Joshi, S. Corde, and W. B. Mori, Phys. Plasmas **27**, 070602 (2020).
[5] W. Wang, K. Feng, L. Ke, C. Yu, Y. Xu, R. Qi, Y. Chen, Z. Qin, Z. Zhang, M. Fang, J. Liu, K. Jiang, H. Wang, C. Wang, X. Yang, F. Wu, Y. Leng, J. Liu, R. Li, and Z. Xu, Nature (London) **595**, 516 (2021).
[6] F. M. Foerster, A. Doepp, F. Haberstroh, K. v. Grafenstein, D. Campbell, Y.-Y. Chang, S. Corde, J. P. Couperus Cabadag, A. Debus, M. F. Gilljohann *et al.*, Phys. Rev. X **12**, 041016 (2022).
[7] W. P. Leemans, B. Nagler, A. J. Gonsalves, C. Toth, K. Nakamura, C. G. Geddes, E. Esarey, C. Schroeder, and S. Hooker, Nat. Phys. **2**, 696 (2006).
[8] H. T. Kim, K. H. Pae, H. J. Cha, I. J. Kim, T. J. Yu, J. H. Sung, S. K. Lee, T. M. Jeong, and J. Lee, Phys. Rev. Lett. **111**, 165002 (2013).
[9] L. T. Ke, K. Feng, W. T. Wang, Z. Y. Qin, C. H. Yu, Y. Wu, Y. Chen, R. Qi, Z. J. Zhang, Y. Xu *et al.*, Phys. Rev. Lett. **126**, 214801 (2021).
[10] A. J. Gonsalves, K. Nakamura, J. Daniels, C. Benedetti, C. Pieronek, T. C. H. de Raadt, S. Steinke, J. H. Bin, S. S. Bulanov, J. van Tilborg *et al.*, Phys. Rev. Lett. **122**, 084801 (2019).
[11] C. B. Schroeder, E. Esarey, C. G. R. Geddes, C. Benedetti, and W. P. Leemans, Phys. Rev. ST Accel. Beams **13**, 101301 (2010).
[12] C. Adolphsen *et al.*, The International Linear Collider Technical Design Report—Volume 3.II: Accelerator Baseline Design, United States: N. p. (2013), 10.2172/1347940.
[13] M. Aicheler, P. Burrows, M. Draper, T. Garvey, P. Lebrun, K. Peach, N. Phinney, H. Schmickler, D. Schulte, and N. Toge (2014), https://www.osti.gov/biblio/1120127.
[14] D. Kaganovicha, A. Ting, D. F. Gordon, R. F. Hubbard, T. G. Jones, A. Ziglerb, and P. Sprangle, Phys. Plasmas **12**, 100702 (2005).
[15] C. Thaury, E. Guillaume, A. Doepp, R. Lehe, A. Lifschitz, K. Ta Phuoc, J. Gautier, J.-P. Goddet, A. Tafzi, A. Flacco *et al.*, Nat. Commun. **6**, 6860 (2015).
[16] C. A. Lindstrom, Phys. Rev. Accel. Beams **24**, 014801 (2021).
[17] S. Steinke, J. Van Tilborg, C. Benedetti, C. Geddes, C. Schroeder, J. Daniels, K. Swanson, A. Gonsalves, K. Nakamura, N. Matlis *et al.*, Nature **530**, 190 (2016).
[18] T. Sokollik, S. Shiraishi, J. Osterhoff, E. Evans, A. J. Gonsalves, K. Nakamura, J. van Tilborg, C. Lin, C. Toth, and W. P. Leemans, AIP Conf. Proc. **1299**, 233 (2010).
[19] J. van Tilborg, S. Steinke, C. G. R. Geddes, N. H. Matlis, B. H. Shaw, A. J. Gonsalves, J. V. Huijts, K. Nakamura, J. Daniels, C. B. Schroeder *et al.*, Phys. Rev. Lett. **115**, 184802 (2015).
[20] J. Luo, M. Chen, W. Y. Wu, S. M. Weng, Z. M. Sheng, C. B. Schroeder, D. A. Jaroszynski, E. Esarey, W. P. Leemans, W. B. Mori *et al.*, Phys. Rev. Lett. **120**, 154801 (2018).
[21] Y. Ehrlich, C. Cohen, A. Zigler, J. Krall, P. Sprangle, and E. Esarey, Phys. Rev. Lett. **77**, 4186 (1996).
[22] A. Zigler, M. Botton, Y. Ferber, G. Johansson, O. Pollak, E. Dekel, F. Filippi, M. Anania, F. Bisesto, R. Pompili *et al.*, Appl. Phys. Lett. **113**, 183505 (2018).
[23] See Supplemental Material at http://link.aps.org/supplemental/10.1103/PhysRevLett.130.215001 for details of capillary fabrication, calibration, installation and setups of experiments and simulations.
[24] K Moore, Zemax opticstudio user manual. Zemax LLC (2017).
[25] F. Bisesto, M. Galletti, E. Chiadroni, and A. Curcio, Opt. Express **26**, 5075 (2018).
[26] A. Bone, N. Lemos, G. Figueira, and J. Dias, J. Phys. D **49**, 155204 (2016).

[27] ANSYS FLUENT 17.0, Theory Guide (2016).
[28] H. Griem, M. Baranger, A. Kolb, and G. Oertel, Phys. Rev. **125**, 177 (1962).
[29] E. Esarey, P. Sprangle, J. Krall, A. Ting, and G. Joyce, Phys. Fluids B **5**, 2690 (1993).
[30] F. Bisesto, M. Galletti, and A. Curcio, Laser Phys. Lett. **17**, 036001 (2020).
[31] R. A. Fonseca, L. O. Silva, F. S. Tsung, V. K. Decyk, W. Lu, C. Ren, W. B. Mori, S. Deng, S. Lee, T. Katsouleas *et al.*, Lect. Notes Comput. Sci. **2331**, 342 (2002).
[32] K. Nakajima, Light **7**, 21 (2018).
[33] J. Palastro, D. Kaganovich, B. Hafizi, Y.-H. Chen, L. Johnson, J. Penano, M. Helle, and A. Mamonau, Phys. Plasmas **24**, 033119 (2017).
[34] M. Chen, J. Luo, F.-Y. Li, F. Liu, Z.-M. Sheng, and J. Zhang, Light **5**, e16015 (2016).
[35] R. Pompili, G. Castorina, M. Ferrario, A. Marocchino, and A. Zigler, AIP Adv. **8**, 015326 (2018).
[36] T. Yang, H. Cheng, Y. Yan, M. Wu, D. Li, Y. Li, Y. Xia, C. Lin, and X. Yan, Phys. Rev. Accel. Beams **24**, 031301 (2021).